Unveiling the mechanisms leading to H_2 production promoted by water decomposition on epitaxial graphene at room temperature

A. Politano[1,*], M. Cattelan[2], D.W. Boukhvalov[3,*], D. Campi[4], A. Cupolillo[1], S. Agnoli[2], N.G. Apostol[5,§], P. Lacovig[5], S. Lizzit[5], D. Farías[6], G. Chiarello[1], G. Granozzi[2], and R. Larciprete[7]

[1] Department of Physics, University of Calabria, via ponte Bucci, 31/C, I-87036 Rende (CS), Italy

[2] Department of Chemical Sciences, University of Padova, via Marzolo 1, I-35131 Padova, Italy

[3] Department of Chemistry, Hanyang University, 17 Haengdang-dong, Seongdong-gu, Seoul 133-791, South Korea

[4] Department of Materials Science, University of Milano-Bicocca, Via R. Cozzi 55, I-20125, Milano, Italy

[5] Elettra-Sincrotrone Trieste S.C.p.A., S.S. 14, Km 163.5, I-34149 Trieste, Italy

[6] Departamento de Física de la Materia Condensada & Instituto de Ciencia de Materiales "Nicolás Cabrera" & Condensed Matter Physics Center (IFIMAC), Universidad Autónoma de Madrid, 28049 Madrid, Spain

[7] CNR, Institute for Complex Systems, Via Fosso del Cavaliere 100, I-00133 Roma, Italy

§ Present address: National Institute of Materials Physics, Atomistilor 105b, 077125 Magurele-Ilfov, Romania.

ABSTRACT

By means of a combination of surface-science spectroscopies and theory, we investigate the mechanisms ruling the catalytic role of epitaxial graphene (Gr) grown on transition-metal substrates for the production of hydrogen from water. Water decomposition at the Gr/metal interface at room temperature provides a hydrogenated Gr sheet, which is buckled and decoupled from the metal substrate. We evaluate the performance of Gr/metal interface as a hydrogen storage medium, with a storage density in the Gr sheet comparable with state-of-the-art materials (1.42 wt.%). Moreover, thermal programmed reaction experiments show that molecular hydrogen can be released upon heating the water-exposed Gr/metal interface above 400 K. The Gr hydro/dehydrogenation process might be exploited for an effective and eco-friendly device to produce (and store) hydrogen from water, i.e. starting from an almost unlimited source.

*corresponding authors: DWB (danil@hanyang.ac.kr) and AP (antonio.politano@fis.unical.it).

Keywords: graphene; water; hydrogen storage; hydrogen production

1 Introduction

Hydrogen represents an alternative eco-friendly and sustainable energy carrier capable of answering the increasing global energy demand.[1-5] The hydrogen economy covers three functional areas: production, storage, and usage. Currently, hydrogen is mainly produced from natural gas via steam reforming [6]. Sustainable alternatives include biological [7] or catalytic [8] degradation of biomass [9] and electrochemical [10] or photochemical water splitting. [11-14] However, some of these processes are unsustainable, since they require a considerable amount of unrenewable energy consumption. For a diffuse usage, energy devices must be compact, [15] combining both fuel production/storage and conversion of primary energy sources into the energy service. A smart solution could be represented by a unique material active for both the production and the storage of hydrogen. Gr is a promising solid-state material for hydrogen storage,[16-18] alternative to metal hydrides[19] and metal-organic frameworks [20, 21] designed to overcome the restrictions of state-of-the-art technologies for hydrogen storage in tanks.[20] An important challenge is represented by the eco-friendly, economic and effective production of clean H_2 fuels from Gr.[16]

Herein, we elucidate the mechanisms which allow the exploitation of Gr/transition-metal interfaces for the production and storage of hydrogen from water. Our model system is Gr/Ni(111) and we adopted both advanced spectroscopic tools and density functional theory (DFT) to clarify the various reaction steps leading to water dissociation at room temperature (RT), whose mechanism is still unclear [22, 23], and to the subsequent hydrogen production.

2 Results and Discussion

The modification of the Gr/Ni(111) interface after the exposure to water at RT has been explored by means of high-resolution X-ray photoelectron spectroscopy (XPS) with synchrotron radiation. The XPS C1s spectrum measured on pristine Gr on Ni(111) (Figure 1a, top) reveals a dominating (C0, 284.84 eV) and a weaker (C1, 284.39 eV) component assigned to strongly interacting and weakly

interacting (in correspondence of rotated domains) graphene on Ni(111),[24] respectively, and/or to the coexistence of top-fcc and bridge-top domains in graphene/Ni(111),[25] plus a minimal additional contribution of Ni carbide [26] (C2, 283.27 eV).

The exposure of Gr to 10^6 L (1 L=$1.33 \cdot 10^{-6}$ mbar·s) of water at RT strongly modifies the C 1s line-shape (Figure 1a, top): the intensity of the originally dominant peak C_0 decreases, the peak C1 disappears and the new components C_3, C4 and C5 emerges at 284.08 eV, 285.30 and 284.31 eV respectively. C3 and C4 are the spectral feature observed after the hydrogenation of Gr/Ni(111)[27], whereas, as it will be clear below, C5 accounts for the graphene regions decoupled from the substrate by water intercalation.

Further information on the water dosed-Gr/Ni(111) interface is obtained by the analysis of the O 1s core-level spectrum (Figure 1b), which shows a main component at 532.51 (O_1) and a second feature at 530.54 eV (O_2). On the basis of results reported in Ref. 28, we assign the two components to undissociated water molecules and to hydroxyl species coming from water dissociation, respectively. It is worth noting that the relative intensity of OH and H2O components is strongly influenced by the interface configuration. Lacking any information about the arrangement of the water molecules below graphene, also in relation to the localization of the OH groups, to estimate the amount of intercalated water and the percentage of dissociated molecules from the O1s component intensities might be misleading .

Significant water-induced effects are also evident in the valence-band spectra shown in Figure 1c. The pristine Gr/Ni(111) is characterized by three features: the intense peak at 1.35 eV is ascribed to Ni 3d bands, while two broad features centered around 6.3 and 9.3 eV are related to $\sigma_{2,3v}$ and π_{1v} valence-band Gr-derived states, respectively. [29] The strong hybridization between $\sigma_{2,3v}$ and π_{1v} states and Ni 3d band induces a BE difference of ~2.4 and ~1 eV, respectively, compared to the corresponding states in graphite. [29] Conversely, the spectrum acquired after water exposure exhibits a band associated to the H_2O-$3a_1$ state at ~7 eV. [30] The attenuated intensity of the valence band in the water-exposed Gr/Ni(111) is due to the presence of chemisorbed species.

To define the configuration of the water-dosed interface, it should be noted that the lack in the C 1s spectrum of spectral features assignable to C-OH bonds, which should arise at ~ 286.5 eV[31] , indicates that the hydroxyl groups are bonded to the Ni substrate. On the other hand, the undissociated water molecules, which do not stick to defect-free Gr nor adsorb on the Ni(111) surface at RT, could be trapped at Gr defect sites or intercalated underneath the Gr cover.

Valuable information about the configuration of surface chemical bonds are provided by the investigation of surface vibrations with high-resolution electron energy loss spectroscopy (HREELS). The vibrational spectrum of H_2O-dosed Gr/Ni(111), shown at the bottom of Figure 1c, exhibits the C-H bending and stretching modes at 179 and 367 meV[32], respectively. The absence of C-OH and O-H vibrations at 65-75 and 410-460 meV [33], respectively, confirms that the OH groups arising from water dissociation are not bound to Gr, which only forms bonds with H atoms. It should be noticed that OH-Ni vibrational modes underneath the Gr cover cannot be probed by the HREELS technique.[34] Similarly, the absence in the vibrational spectra of modes coming from undissociated water molecules (for H_2O vibrational spectrum, see Figure S4 in the Supporting Information, SI) demonstrates that the H_2O molecules, detected in the O 1s spectrum in Figure 1b, have penetrated below Gr.

Therefore, the scenario emerging from our results is that water molecules interacting with the Gr/Ni(111) interface intercalate below Gr and partly dissociate, leading to H atoms bonded to Gr and OH groups bonded to the metal substrate. This is expected to result into an increased Gr-Ni distance and into the buckling of the Gr sheet (see Figure 3 and its description), as a consequence of the hydrogenation-induced modification in the hybridization from sp^2 to sp^3.[35] Accordingly, the DFT calculations of core-level shifts for C 1s for Gr decoupled from the Ni substrate by the presence of intercalated species indicate a notable down-shift of ~0.7 eV (see Figure S5 in the SI), in agreement with the behavior observed in Figure 1a.

The thermal stability of the water-dosed Gr/Ni(111) interface was probed by monitoring the C 1s spectra by means of fast-XPS experiments performed in real time during sample heating. The

sequence of C 1s spectra is shown as a 2D plot in Figure 2a, whereas Figure 2b reports the intensity of the different C 1s spectral components. Thermal annealing at 350 K starts to convert C_3 and C_4 into C_0. In the high resolution C1s spectrum taken on the sample heated at 470 K (see SI, Fig.S5), C3 has vanished and C0 and C1 has recovered most of their initial intensity after complete hydrogen desorption, whereas the extra intensity at ~ 284.3 in correspondence of C5 still reveals the presence of intercalated water. After annealing to 770 K the C 1s spectrum has fully recovered the line-shape and intensity of the pristine Gr on Ni(111). The C 1s spectra measured on Gr/Ni(111) before exposure to water and after sample heating of the water-dosed system are compared in the inset of Figure 2b. Their perfect similarity leads us to conclude that the Gr hydro/dehydrogenation process does not induce any structural damage of the Gr lattice, It is worth noting that whereas defected Gr/Ru(0001) exposed to water is dramatically split, defect-free graphene remains intact, and Gr/Cu(111) is only occasionally damaged.[36] Accordingly, our results demonstrate the stability of Gr/Ni(111) exposed to water and the perfect process reversibility.

A similar evolution of the water-dosed Gr/Ni(111) interface with the temperature is illustrated by HREELS spectra (Figure 2c), which show that above 300 K the intensity of C-H vibrations decreases progressively and finally vanishes at ~440 K. In the thermal evolution of the O 1s spectrum (Figure 2d), the behavior of the intensity of O_1 and O_2 components (defined in Figure 1b) indicates a different evolution for the OH and H_2O species present at the Gr/Ni(111) interface. The progressive decrease of the O_1 component, which starts at 400 K and proceeds up to 700 K, in parallel with the C5 component of the C1s spectrum, confirms that the H_2O molecules are entrapped underneath the Gr cover. The increasing temperature allows them to diffuse and desorb, likely passing through grain boundaries and defects of the Gr lattice. By contrast, the constant intensity of the O_2 peak ascribed to OH groups attests the higher thermal stability up to 750 K of the OH-Ni bonds.

The various physicochemical processes involving water intercalated underneath Gr were modelled by DFT calculations (Figure 3).. Grain boundaries are the main route for the penetration

of water between Gr and the metal substrate in agreement with the results reported for the intercalation of atoms[37]and molecules[38] below graphene. Water intercalation at RT requires high partial pressure (i.e. ~10^{-3} mbar, see Methods), as also found for CO intercalation at RT in Gr/metals.[39,40] The next step of our DFT survey is the modelling of H_2O decomposition at the Gr/metal interface. We considered the decomposition of two water molecules, which can occur through different paths, leading to the following possible configurations: (*a*) two H atoms adsorbed on Gr and two OH groups on the metal substrate (Figure 3b); (*b*) both OH groups on Gr and both H atoms on the metal; (*c*) one H and one OH on Gr and the same water fragments on the metal; (*d*) all H and OH on Gr or (*e*) all H and OH on the substrate. Our calculations indicate that the configurations (*d*) and (*e*), where all fragments are on Gr or on Ni, are less energetically favorable by about 1.5 eV than the first reaction path leading to hydrogenation of Gr and OH chemisorption on the Ni surface. Moreover, the (*b*) and (*c*) configurations are less favorable than the (*a*), although only by 0.2 eV. Thus, our DFT calculations confirm that the most energetically favorable reaction path for the decomposition of two water molecules intercalated below Gr/Ni(111) will provide hydrogenated Gr and hydroxyl groups bonded to the substrate. As shown in Figure 3, for defect-free Gr this process is endothermic,. However the presence of SW defects decreases the chemisorption energy and the molecular dissociation becomes exhothermic. Then the role of the Stone Wales defects is to increase the chemical reactivity of graphene as it has been predicted to happen in the hydrogenation of free standing graphene. [41]

Then, we have evaluated the stability of the H atoms on Gr with respect to the migration to the underlying metal substrate by modelling a two-stage process: desorption of first (Figure 3c) and, successively, of the second (Figure 3d) H atom. For defect-free Gr or for Gr with a low density of Stone-Wales defects, the migration to the substrate of even a single hydrogen atom is exothermic. This result is somehow unexpected, since the presence of an odd number of monovalent species chemisorbed on Gr should be energetically unfavorable with respect to the presence of an even number of monovalent species.[42] The destabilization in the chemical bond consequent to single-

atom desorption is compensated through the occurrence of charge transfer from the substrate[43], which makes the H migration to the metal substrate energetically convenient. When increasing the density of Stone-Wales defects at the surface, the permanence of both H atoms on Gr becomes definitely favorable, because of the stabilizing effect of chemisorbed species, which is proportional to the number of defects.

Desorption of the second H atom from Gr (Figure 3d) is energetically favorable uniquely for defect-free Gr and only in this case the H_2 molecule spontaneously forms in the space between Gr and substrate. In the presence of defects, the migration of both hydrogen atoms to the substrate has an energy cost and, thus, the formation of H dimers on the metal substrate is unfavorable without providing external energy.

Thus, DFT calculations demonstrate that, close to the Gr grain boundaries, water molecules decompose to hydrogen and hydroxyl groups and stable hydrogenation of Gr occurs. The amount of hydrogenated Gr and the configuration of the hydrogenated patterns strongly depend on the atomic structure of Gr defects at the grain boundaries. However, the Ni substrate reduces the barrier for water decomposition by more than 0.5 eV with respect to pristine free-standing, defect-free Gr.

After the elucidation of the reaction scenario, it is mandatory to evaluate the amount of hydrogen which is possible to store at the Gr/Ni(111) interface. To this aim, we probed the species evolving from the water-dosed Gr/Ni(111) interface upon thermal annealing by temperature programmed reaction (TPR). The primary role of Gr in the H_2O dissociation was evidenced by carrying out also a parallel experiment on the bare Ni(111) surface. To avoid any possible contribution due to the H_2 background in the ultra-high vacuum (UHV) chamber, we have conducted this experiment by dosing D_2O. Bare Ni(111) and Gr/Ni(111) surfaces were exposed to saturation doses of D_2O at RT and the TPR curves were measured while heating the samples at rate of 2 K/s (Figure 4a,b). In the case of Gr/Ni(111), the D_2O, D_2, O_2 and O TPR profiles shown in Figure 4b indicate that D_2 is the unique desorbing species.. The D_2 desorption peak from Gr/Ni(111) centered at 442 K, corresponding to an activation energy of ~1.0 eV, is followed by a secondary

peak at 643 K, corresponding to an activation energy of ~1.6 eV. These results are in fair agreement with thermal programmed desorption experiments carried out on H-dosed Gr/Ni(111).[44]

We want to point out that it is not possible to observe the desorption of D2O during thermal annealing of D2O-dosed Gr/ Ni(111) since the very high background signal of D2O, arising from the large dose, makes D2O desorption hardly discernible. On the other hand, the absence of a well-distinct desorption peak for D2O is also in agreement with the XPS measurements reported in Figure 2d, where the O1 component of the O 1s core level only gradually decreases above 400 K as a function of temperature.

By contrast, D2 production from the D2O-dosed Ni(111) is not an effective process, as demonstrated by the vanishing D2 TPR curve shown in Figure 4b.To further prove the occurrence of water dissociation at the Gr/Ni(111) surface at RT, we have also conducted TPR experiments with H_2O/D_2O mixtures. In this case, the observation of HD molecules, resulting from the recombination of H and D fragments, demonstrates the RT dissociation of both H_2O and D_2O at the Gr/Ni(111) interface.

The amount of D_2 evolving from the Gr/Ni(111) interface saturated at RT with water molecules was evaluated by calibrating the D_2 TPR curve, shown in Figure 4b, with the H_2 yield from the Ni(111) surface hydrogenated at 150 K up to a H saturation coverage of 0.5 ML_{Ni}. We remind that 1 ML_{Ni} corresponds to a surface atomic density of $1.86x10^{15}$ atoms/cm^2. The thermal programmed desorption H_2 curve, obtained from the H/Ni(111) surface and reported in Figure 4c, shows the β_2 desorption peak at 367 K and a second peak at 320 K related to the β_1 states.[45] By using the integrated intensities of this curve to normalize the D_2 TPR curve of Figure 4b, it results that the amount of D_2 evolving from water-saturated Gr/Ni(111) corresponds to 0.17 ML_{Gr} ($1ML_{Gr}=2ML_{Ni}$).

From the quantitative analysis of the TPR data, we can thus assert that the gravimetric density of the hydrogenated Gr reachable in water-dosed Gr/Ni(111) interfaces is 1.42 wt.% at RT and in UHV

conditions. As a comparison, $LaNi_5$, a typical metal alloy forming hydrides, shows a gravimetric density of 1.37 wt. % [46] at RT. It is expected that decoration of Gr by Ca[47] or transition-metal atoms[48] and, moreover, the substitutional doping of Gr by N[48] or B[49] could further increase the gravimetric capacity.

3 Conclusions

By means of a combination of advanced spectroscopic techniques and theory, we have elucidated the mechanism leading to water decomposition at the Gr/metal interfaces at RT, resulting in hydrogenated Gr, with a gravimetric density competitive with current technology for H storage. Molecular hydrogen is produced by heating above 400 K. Our results represent a crucial milestone in the technological road map for the use of Gr/metal interfaces in catalysis and in energy-related applications.

Methods

Sample growth

The sample was a Ni(111) single crystal. The substrate was cleaned by repeated cycles of ion sputtering and annealing at 1050 K. Gr growth was carried out by dosing ethylene with the sample kept at 790 K, while monitoring in real time the C 1s line-shape (SI, Figure S1). The Gr overlayer quality is good, as indicated by the intense spots recorded in the He-atom diffraction pattern (SI, Figure S2).

Spectroscopic investigations were performed in four different UHV chambers in Trieste, Padova, Rende, and Madrid.

Exposure to water

Water was dosed at RT on a Gr/Ni(111) surface through a doser. The doser is a Mo tube with diameter 6 mm, placed almost in contact with the sample in order to enhance the local pressure. In these conditions, we reached a partial water pressure of 10^{-3} mbar on the sample. We dosed water up to a total exposure of 10^{6} L. Such a high dose is motivated by the low sticking coefficient of water molecules at RT on Gr/Ni(111) (see SI, section S3)

X-ray photoelectron spectroscopy (XPS)

High-resolution XPS experiments were performed in the UHV chamber of the SuperESCA beam line of the synchrotron radiation source Elettra (Trieste, Italy). High-resolution C 1s and O 1s core-level spectra were measured at a photon energy of 400 and 650 eV, respectively, with an overall energy resolution ranging from 40 to 150 meV. Valence-band spectra were acquired with a photon energy of 135 eV. For each spectrum, the BE was calibrated with the Fermi level position of the Ni substrate. The measurements were performed with the photon beam impinging at grazing incidence (70°), while photoelectrons were collected at normal emission angle. The core-level spectra were best fitted with Doniach-Šunjić functions convoluted with Gaussians, and a linear background.

High-resolution electron energy loss spectroscopy (HREELS)

HREELS experiments were performed by using an electron energy loss spectrometer (Delta 0.5, SPECS) at University of Calabria, Rende (CS), Italy. The energy resolution of the spectrometer is 5 meV. The primary electron beam energy is 4 eV. Each spectrum was normalized to the intensity of the elastic peak. HREELS spectra were acquired in specular conditions, with incident and scattering angles of 55° with respect to the surface normal.

Temperature-programmed reaction (TPR)

TPR was measured with a HIDEN HAL 301 PIC quadrupole mass spectrometer with an electron multiplier detector at University of Padova, Italy. To analyze the desorption species coming only from the sample surface, the quadrupole filter, covered by a quartz shield holding a 8 mm hole in correspondence to the sample, was placed at 5 mm from the Ni(111) single crystal, which was

mounted on two tantalum wires. A linear heating ramp of 2 K/s was used. The base pressure during the experiments was better than $6 \cdot 10^{-10}$ mbar.

DFT calculations

We used DFT, as implemented in the pseudopotential code SIESTA.[50] All calculations were performed using the generalized gradient approximation (GGA-PBE) with spin-polarization[51] and implementation of the correction of van der Waals forces.[52] All calculations were carried out with an energy mesh cut-off of 360 Ry and a k-point mesh of 8×6×2 in the Monkhorst-Pack scheme.[53]

We used a rectangular supercell of 48 carbon atoms over metallic slab containing four layers (24 Ni atoms in each layer). During the optimization, the ion cores were described by norm-conserving non-relativistic pseudo-potentials[53] with cut-off radii 1.14, 1.45, 1.25, 2.15 a.u. for C, O, H and Ni, respectively, and the wave-functions were expanded with localized orbitals and double-ζ basis set for hydrogen and a double-ζ plus polarization basis set for other species. Full optimization of the atomic positions was performed. Optimization of the force and total energy was carried out with an accuracy of 0.04 eV/Å and 1 meV, respectively.

For modelling grain boundaries between Gr domains, we used Gr with different amount of Stone-Wales defects (see Fig 4a). The intercalation energy was calculated by:

$E_{intercalation} = E_{system+2H2O} - (E_{system} + 2E_{H2O})/m$

where E_{system} and $E_{system+2H2O}$ are the total energy of Gr on metallic substrate before and after the intercalation of two water molecules, respectively; E_{H2O} is the total energy of water molecule and m is the number of carbon atoms in the supercell.

The optimized distance between the metal substrate and Gr obtained in our calculations agrees with experimental values in literature (see discussion in Ref. 54).

Associated content

This material is available free of charge via the Internet at http:// pubs.acs.org.

1) Real-time growth of Gr on Ni(111);
2) Evaluation of the crystalline quality of the grown Gr layer by He-atom scattering (HAS);
3) Sticking coefficient of water on Gr/Ni(111) at RT;
4) Ice formation and desorption in Gr/metals;
5) Calculations of core-level shifts;
6) DFT model on water dissociation at RT in Gr/metals.

Acknowledgments

AP and GC thank Fabio Vito for technical support. AP and RL thank Elettra Sincrotrone Trieste S.C.p.A. for financial support. RL acknowledges the support by MIUR through the program "Progetto Premiale 2012" - Project ABNANOTECH. SA, MC and GG acknowledge Italian MIUR through the national grant Futuro in Ricerca 2012 RBFR128BEC "Beyond graphene: tailored C-layers for novel catalytic materials and green chemistry" and by the University of Padova funded project: CPDA128318/12 "Study of the catalytic activity of complex graphene nanoarchitectures from ideal to real conditions". DF acknowledges European Union (FP7): Theme NMP.2012.1.4-3 Grant no. 309672.

Author information

The authors declare no competing financial interests.

REFERENCES AND NOTES

1. Satyapal, S.; Petrovic, J.; Read, C.; Thomas, G.; Ordaz, G., The U.S. Department of Energy's National Hydrogen Storage Project: Progress towards meeting hydrogen-powered vehicle requirements. *Catal. Today* **2007,** *120*, 246-256.
2. McAteer, D.; Gholamvand, Z.; McEvoy, N.; Harvey, A.; O'Malley, E.; Duesberg, G. S.; Coleman, J. N., Thickness Dependence and Percolation Scaling of Hydrogen Production Rate in MoS_2 Nanosheet and Nanosheet–Carbon Nanotube Composite Catalytic Electrodes. *ACS Nano* **2016**, doi:10.1021/acsnano.5b05907.
3. Duan, J.; Chen, S.; Jaroniec, M.; Qiao, S. Z., Porous C_3N_4 Nanolayers@N-Graphene Films as Catalyst Electrodes for Highly Efficient Hydrogen Evolution. *ACS Nano* **2015,** *9*, 931-940.
4. Fan, X.; Peng, Z.; Ye, R.; Zhou, H.; Guo, X., M_3C (M: Fe, Co, Ni) Nanocrystals Encased in Graphene Nanoribbons: An Active and Stable Bifunctional Electrocatalyst for Oxygen Reduction and Hydrogen Evolution Reactions. *ACS Nano* **2015,** *9*, 7407-7418.
5. Ting, V. P.; Ramirez-Cuesta, A. J.; Bimbo, N.; Sharpe, J. E.; Noguera-Diaz, A.; Presser, V.; Rudic, S.; Mays, T. J., Direct Evidence for Solid-like Hydrogen in a Nanoporous Carbon Hydrogen Storage Material at Supercritical Temperatures. *ACS Nano* **2015,** *9*, 8249-8254.
6. Liguras, D. K.; Kondarides, D. I.; Verykios, X. E., Production of hydrogen for fuel cells by steam reforming of ethanol over supported noble metal catalysts. *Appl. Catal., B: Environ.* **2003,** *43*, 345-354.
7. Das, D.; Veziroğlu, T. N., Hydrogen production by biological processes: a survey of literature. *Int. J. Hydrogen Energy* **2001,** *26*, 13-28.

8. Cortright, R. D.; Davda, R. R.; Dumesic, J. A., Hydrogen from catalytic reforming of biomass-derived hydrocarbons in liquid water. *Nature* **2002,** *418*, 964-967.
9. Kim, M.-S.; Baek, J.-S.; Yun, Y.-S.; Jun Sim, S.; Park, S.; Kim, S.-C., Hydrogen production from Chlamydomonas reinhardtii biomass using a two-step conversion process: Anaerobic conversion and photosynthetic fermentation. *Int. J. Hydrogen Energy* **2006,** *31*, 812-816.
10. Doyle, R. L.; Godwin, I. J.; Brandon, M. P.; Lyons, M. E. G., Redox and electrochemical water splitting catalytic properties of hydrated metal oxide modified electrodes. *Phys. Chem. Chem. Phys.* **2013,** *15*, 13737-13783.
11. Bak, T.; Nowotny, J.; Rekas, M.; Sorrell, C. C., Photo-electrochemical hydrogen generation from water using solar energy. Materials-related aspects. *Int. J. Hydrogen Energy* **2002,** *27*, 991-1022.
12. Kment, S.; Schmuki, P.; Hubicka, Z.; Machala, L.; Kirchgeorg, R.; Liu, N.; Wang, L.; Lee, K.; Olejnicek, J.; Cada, M.; Gregora, I.; Zboril, R., Photoanodes with Fully Controllable Texture: The Enhanced Water Splitting Efficiency of Thin Hematite Films Exhibiting Solely (110) Crystal Orientation. *ACS Nano* **2015,** *9*, 7113-7123.
13. Chen, Y.; Tran, P. D.; Boix, P.; Ren, Y.; Chiam, S. Y.; Li, Z.; Fu, K.; Wong, L. H.; Barber, J., Silicon Decorated with Amorphous Cobalt Molybdenum Sulfide Catalyst as an Efficient Photocathode for Solar Hydrogen Generation. *ACS Nano* **2015,** *9*, 3829-3836.
14. Steier, L.; Luo, J.; Schreier, M.; Mayer, M. T.; Sajavaara, T.; Grätzel, M., Low-Temperature Atomic Layer Deposition of Crystalline and Photoactive Ultrathin Hematite Films for Solar Water Splitting. *ACS Nano* **2015,** *9*, 11775-11783.
15. Tozzini, V.; Pellegrini, V., Prospects for hydrogen storage in graphene. *Phys. Chem. Chem. Phys.* **2013,** *15*, 80-89.
16. Bonaccorso, F.; Colombo, L.; Yu, G.; Stoller, M.; Tozzini, V.; Ferrari, A. C.; Ruoff, R. S.; Pellegrini, V., Graphene, related two-dimensional crystals, and hybrid systems for energy conversion and storage. *Science* **2015,** *347*, 1246501.
17. Balog, R.; Andersen, M.; Jørgensen, B.; Sljivancanin, Z.; Hammer, B.; Baraldi, A.; Larciprete, R.; Hofmann, P.; Hornekær, L.; Lizzit, S., Controlling Hydrogenation of Graphene on Ir(111). *ACS Nano* **2013,** *7*, 3823–3832.
18. Kumar, R.; Oh, J.-H.; Kim, H.-J.; Jung, J.-H.; Jung, C.-H.; Hong, W. G.; Kim, H.-J.; Park, J.-Y.; Oh, I.-K., Nanohole-Structured and Palladium-Embedded 3D Porous Graphene for Ultrahigh Hydrogen Storage and CO Oxidation Multifunctionalities. *ACS Nano* **2015,** *9*, 7343-7351.
19. Sakintuna, B.; Lamari-Darkrim, F.; Hirscher, M., Metal hydride materials for solid hydrogen storage: A review. *Int. J. Hydrogen Energy* **2007,** *32*, 1121-1140.
20. Jena, P., Materials for Hydrogen Storage: Past, Present, and Future. *J. Phys. Chem. Lett.* **2011,** *2*, 206-211.
21. Murray, L. J.; Dinca, M.; Long, J. R., Hydrogen storage in metal-organic frameworks. *Chem. Soc. Rev.* **2009,** *38*, 1294-1314.
22. Politano, A.; Chiarello, G., Periodically rippled graphene on Ru(0001): A template for site-selective adsorption of hydrogen dimers via water splitting and hydrogen-spillover at room temperature. *Carbon* **2013,** *61*, 412-417.
23. Politano, A.; Marino, A. R.; Formoso, V.; Chiarello, G., Water adsorption on graphene/Pt(111) at room temperature: A vibrational investigation. *AIP Advances* **2011,** *1*, 042130.
24. Patera, L. L.; Africh, C.; Weatherup, R. S.; Blume, R.; Bhardwaj, S.; Castellarin-Cudia, C.; Knop-Gericke, A.; Schloegl, R.; Comelli, G.; Hofmann, S.; C. Cepek, *I*n Situ Observations of the Atomistic Mechanisms of Ni Catalyzed Low Temperature Graphene Growth, *ACS Nano* **2013**, 7, 7901–7912.
25 Zhao, W.; Kozlov, S. M.; Höfert, O.; Gotterbarm, K.; Lorenz, M. P. A.; Viñes, F.; Papp, C.; Görling, A.; Steinrück, H.-P., Graphene on Ni(111): Coexistence of Different Surface Structures. *J. Phys. Chem. Lett.* **2011,** *2*, 759-764.
26. Grüneis, A.; Kummer, K.; Vyalikh, D. V., Dynamics of graphene growth on a metal surface: A time-dependent photoemission study. *New J. Phys.* **2009,** *11*, 073050.

27. Ng, M. L.; Balog, R.; Hornekær, L.; Preobrajenski, A. B.; Vinogradov, N. A.; Mårtensson, N.; Schulte, K., Controlling Hydrogenation of Graphene on Transition Metals. *J. Phys. Chem. C* **2010,** *114*, 18559-18565.
28. Yamamoto, S.; Bluhm, H.; Andersson, K.; Ketteler, G.; Ogasawara, H.; Salmeron, M.; Nilsson, A., In situ x-ray photoelectron spectroscopy studies of water on metals and oxides at ambient conditions. *J. Phys.: Condens. Matter* **2008,** *20*, 184025.
29. Weser, M.; Rehder, Y.; Horn, K.; Sicot, M.; Fonin, M.; Preobrajenski, A. B.; Voloshina, E. N.; Goering, E.; Dedkov, Y. S., Induced magnetism of carbon atoms at the graphene/Ni(111) interface. *Appl. Phys. Lett.* **2010,** *96*, 012504.
30. Böttcher, S.; Weser, M.; Dedkov, Y.; Horn, K.; Voloshina, E.; Paulus, B., Graphene on ferromagnetic surfaces and its functionalization with water and ammonia. *Nanoscale Res. Lett.* **2011,** *6*, 214.
31. Hunt, A.; Dikin, D. A.; Kurmaev, E. Z.; Boyko, T. D.; Bazylewski, P.; Chang, G. S.; Moewes, A., Epoxide Speciation and Functional Group Distribution in Graphene Oxide Paper-Like Materials. *Adv. Funct. Mater.* **2012,** *22*, 3950-3957.
32. Kim, H.; Balgar, T.; Hasselbrink, E., The stretching vibration of hydrogen adsorbed on epitaxial graphene studied by sum-frequency generation spectroscopy. *Chem. Phys. Lett.* **2011,** *508*, 1-5.
33. Henderson, M. A., The interaction of water with solid surfaces: fundamental aspects revisited. *Surf. Sci. Rep.* **2002,** *46*, 1-308.
34. Politano, A.; Chiarello, G.; Benedek, G.; Chulkov, E. V.; Echenique, P. M., Vibrational measurements on alkali coadsorption systems: experiments and theory. *Surf. Sci. Rep.* **2013,** *68*, 305–389.
35. Elias, D. C.; Nair, R. R.; Mohiuddin, T. M. G.; Morozov, S. V.; Blake, P.; Halsall, M. P.; Ferrari, A. C.; Boukhvalov, D. W.; Katsnelson, M. I.; Geim, A. K.; Novoselov, K. S., Control of graphene's properties by reversible hydrogenation: Evidence for graphane. *Science* **2009,** *323*, 610-613.
36. Feng, X.; Maier, S.; Salmeron, M., Water splits epitaxial graphene and intercalates. *J. Am. Chem. Soc.* **2012,** *134*, 5662–5668.
37. Petrović, M.; Šrut Rakić, I.; Runte, S.; Busse, C.; Sadowski, J. T.; Lazić, P.; Pletikosić, I.; Pan, Z. H.; Milun, M.; Pervan, P.; Atodiresei, N.; Brako, R.; Šokčević, D.; Valla, T.; Michely, T.; Kralj, M., The mechanism of caesium intercalation of graphene. *Nat. Commun.* **2013,** *4*, 2772.
38 Yao
39. Jin, L.; Fu, Q.; Dong, A.; Ning, Y.; Wang, Z.; Bluhm, H.; Bao, X., Surface Chemistry of CO on Ru(0001) under the Confinement of Graphene Cover. *J. Phys. Chem. C* **2014,** *118*, 12391–12398.
40. Wei, M.; Fu, Q.; Yang, Y.; Wei, W.; Crumlin, E.; Bluhm, H.; Bao, X., Modulation of Surface Chemistry of CO on Ni(111) by Surface Graphene and Carbidic Carbon. *J. Phys. Chem. C* **2015,** *119*, 13590-13597.
41. Boukhvalov, D. W.; Katsnelson, M. I., Chemical Functionalization of Graphene with Defects. *Nano Lett.* **2008,** *8*, 4373-4379.
42. Galakhov, V. R.; Buling, A.; Neumann, M.; Ovechkina, N. A.; Shkvarin, A. S.; Semenova, A. S.; Uimin, M. A.; Yermakov, A. Y.; Kurmaev, E. Z.; Vilkov, O. Y.; Boukhvalov, D. W., Carbon States in Carbon-Encapsulated Nickel Nanoparticles Studied by Means of X-ray Absorption, Emission, and Photoelectron Spectroscopies. *J. Phys. Chem. C* **2011,** *115*, 24615-24620.
43. Boukhvalov, D. W.; Son, Y. W.; Ruoff, R. S., Water Splitting over Graphene-Based Catalysts: Ab Initio Calculations. *ACS Catalysis* **2014,** *4*, 2016-2021.
44. Zhao, W.; Gebhardt, J.; Späth, F.; Gotterbarm, K.; Gleichweit, C.; Steinrück, H.-P.; Görling, A.; Papp, C., Reversible Hydrogenation of Graphene on Ni(111)—Synthesis of “Graphone”. *Chem. Eur. J.* **2015,** *21*, 3347-3358.
45 Russell, J. N.; Gates, S. M.; Yates, J. T., Isotope effects in hydrogen adsorption on Ni(111): Direct observation of a molecular precursor state. *J. Chem. Phys.* **1986,** *85*, 6792-6802.
46. Schlapbach, L.; Züttel, A., Hydrogen-storage materials for mobile applications. *Nature* **2001,** *414*, 353-358.
47. Lee, H.; Ihm, J.; Cohen, M. L.; Louie, S. G., Calcium-Decorated Graphene-Based Nanostructures for Hydrogen Storage. *Nano Lett.* **2010,** *10*, 793-798.
48. Parambhath, V. B.; Nagar, R.; Ramaprabhu, S., Effect of Nitrogen Doping on Hydrogen Storage Capacity of Palladium Decorated Graphene. *Langmuir* **2012,** *28*, 7826-7833.

49. Beheshti, E.; Nojeh, A.; Servati, P., A first-principles study of calcium-decorated, boron-doped graphene for high capacity hydrogen storage. *Carbon* **2011,** *49*, 1561-1567.
50. Soler, J. M.; Artacho, E.; Gale, J. D.; García, A.; Junquera, J.; Ordejón, P.; Sánchez-Portal, D., The SIESTA method for ab initio order- N materials simulation. *J. Phys.: Condens. Matter* **2002,** *14*, 2745.
51. Perdew, J. P.; Burke, K.; Ernzerhof, M., Generalized Gradient Approximation Made Simple. *Phys. Rev. Lett.* **1996,** *77*, 3865-3868.
52. Román-Pérez, G.; Soler, J. M., Efficient Implementation of a van der Waals Density Functional: Application to Double-Wall Carbon Nanotubes. *Phys. Rev. Lett.* **2009,** *103*, 096102.
53. Troullier, N.; Martins, J. L., Efficient pseudopotentials for plane-wave calculations. *Phys. Rev. B* **1991,** *43*, 1993-2006.
54. Boukhvalov, D. W.; Gornostyrev, Y. N.; Uimin, M. A.; Korolev, A. V.; Yermakov, A. Y., Atomic, electronic and magnetic structure of graphene/iron and nickel interfaces: theory and experiment. *RSC Advances* **2015,** *5*, 9173-9179.
54.

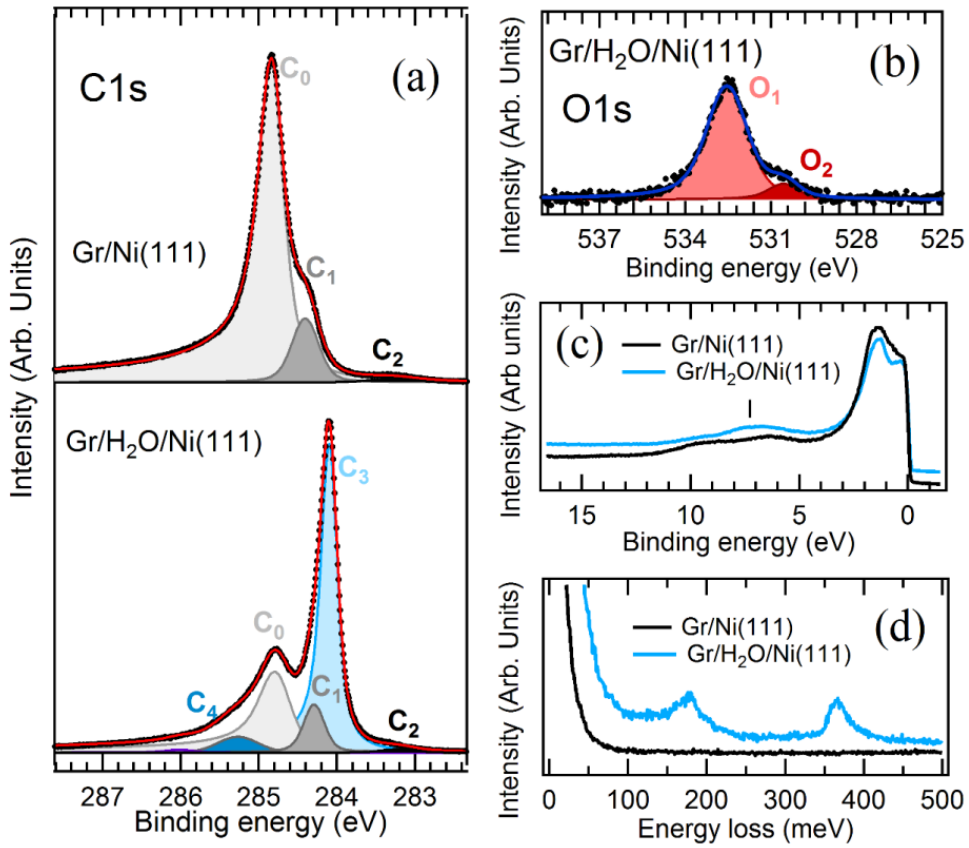

Figure 1. XPS and vibrational investigation of pristine and water-exposed Gr. (a) C 1s core-level spectra in pristine Gr/Ni(111) (top panel) and H_2O-exposed Gr/Ni(111) (bottom panel), measured with photon energy of 400 eV. The assignment of C_0, C_1, C_3 and C_4 peaks is described in the main text. By contrast, C_2 is a residual carbide species.[54] **(b)** O 1s core-level spectrum in H_2O-exposed Gr/Ni(111). The photon energy is 650 eV. **(c)** Valence-band spectra in pristine (black curve) and H_2O-expoxed Gr/Ni(111) (blue curve). Spectra have been shifted for clarity. The photon energy is 135 eV. **(d)** Vibrational spectrum, measured by HREELS in specular scattering conditions for pristine (black curve) and H_2O-expoxed Gr/Ni(111) (blue curve). The primary electron beam energy is 4 eV.

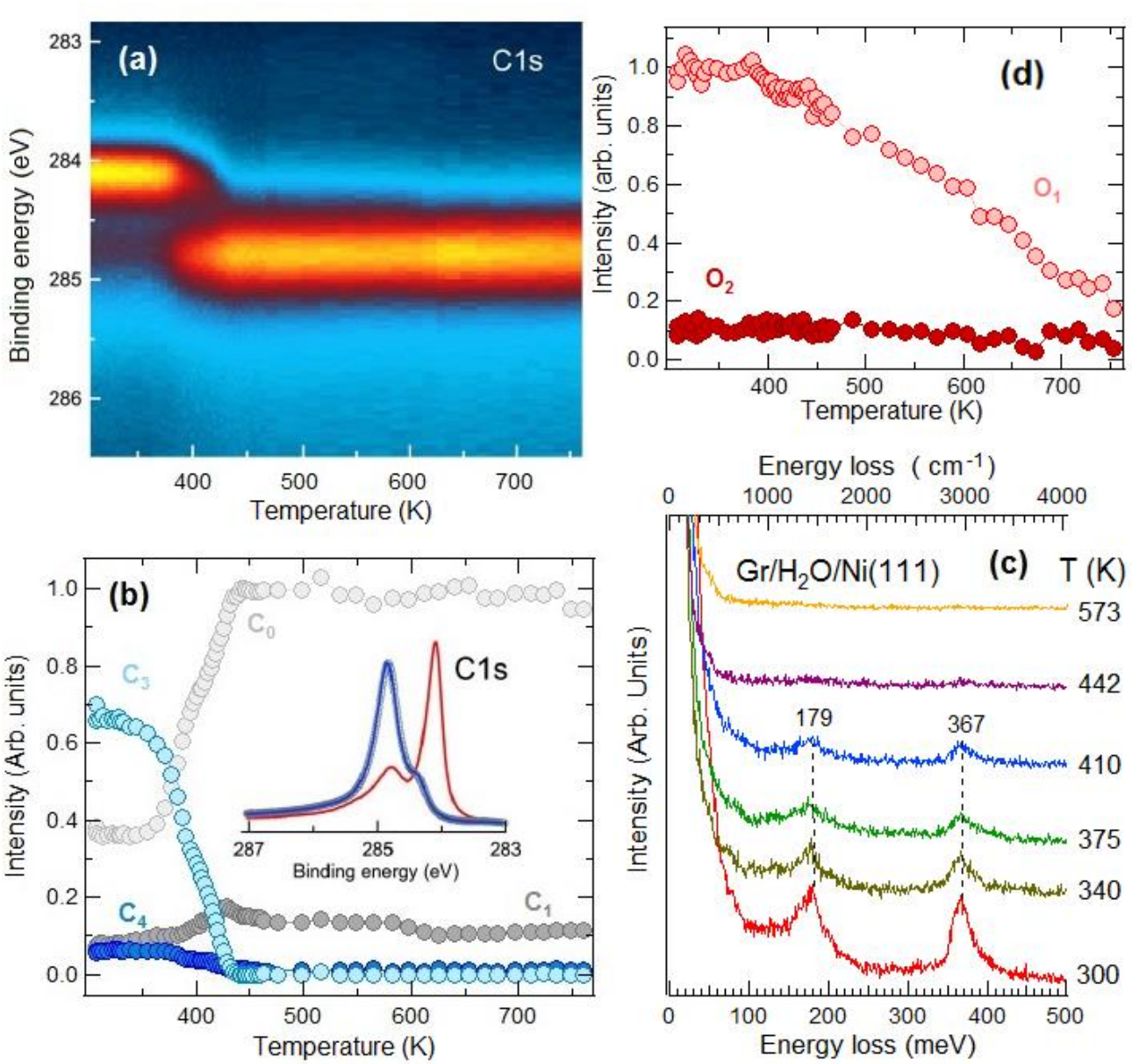

Figure 2. Desorption of water fragments from Gr. (a) Real-time evolution of the C 1s signal in H_2O-exposed Gr/Ni(111) during the heating at a rate of 0.4 K/s. **(b)** Intensity of the various components of the C 1s core-level spectrum. Each peak has been labeled as in Figure 1a. The inset shows the C 1s signal recorded for Gr/Ni(111) (grey circles), H_2O-dosed Gr/Ni(111) (red curve) and after heating to 442 K (blue curve). **(c)** Vibrational spectrum measured by HREELS for the H_2O-modified Gr/Ni(111) surface, annealed to different values of temperature. The bottom axis reports vibrational energies in meV, while the corresponding values in cm^{-1} are shown in the top axis. **(d)** Intensity of the O_1 and O_2 components (see Figure 1b) in O 1s spectra recorded in real time during the heating of the water-exposed Gr/Ni(111) from 300 up to 750 K. The intensities have been obtained by fitting the O 1s spectra with two Voigt line-shapes after background subtraction.

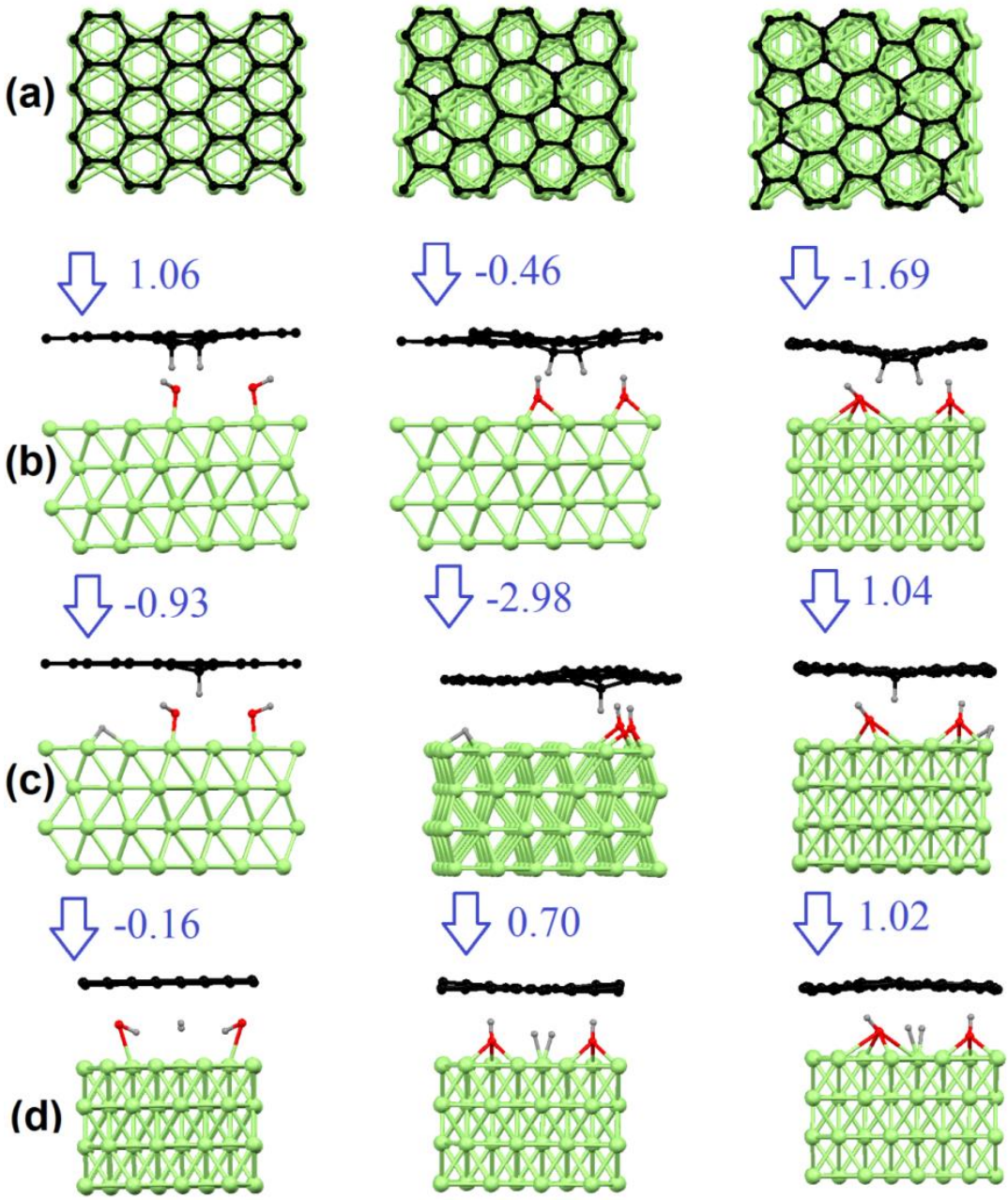

Figure 3. DFT model on water-induced hydrogenation of Gr/metals. Optimized atomic structures of Gr without (left column) and with various amount of defects (central and right columns) for: **(a)** Gr/Ni(111); **(b**) intercalation of two water molecules, which decompose into hydroxyl groups bonded to the Ni substrate and hydrogen atoms covalently bonded to Gr; migration

of one **(c)** and two **(d)** hydrogen atoms from Gr to the metal substrate. Numbers correspond to the energetic values (in eV) of the various processes.

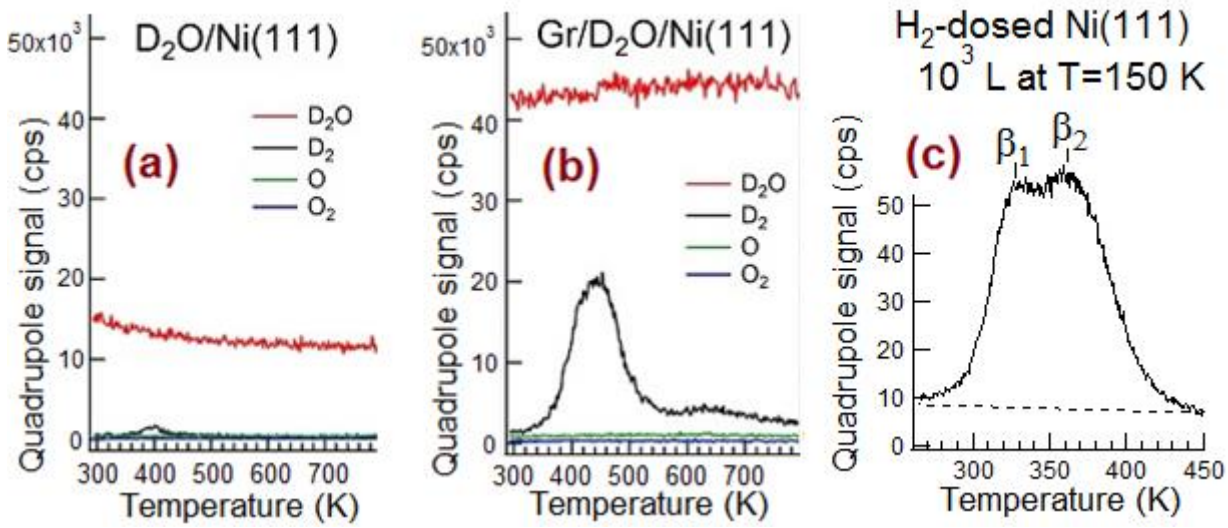

Figure 4. D_2 production from D_2O. TPR spectra acquired for the D_2O-exposed Ni(111) and Gr/Ni(111) surfaces are reported in panels **(a)** and **(b)**, respectively. The evolution of D_2O (red curve), D_2 (black curve), atomic O (green curve) and O_2 (blue curve) has been recorded. The weak D_2 desorption peak from Ni(111) is caused by residual deuterium in the water flask. **(c)** Thermal programmed desorption spectra of the H_2-dosed Ni(111) surface acquired using a 2 K/s heating rate.

Supporting Information

Unveiling the Mechanisms Leading to H_2 Production promoted by Water Decomposition on Epitaxial Graphene at Room Temperature

Antonio Politano, Mattia Cattelan, Danil W. Boukhvalov, Davide Campi, Anna Cupolillo, Stefano Agnoli, Nicoleta G. Apostol, Paolo Lacovig, Silvano Lizzit, Daniel Farías, Gennaro Chiarello, Gaetano Granozzi, and Rosanna Larciprete

Index

S1. Real-time growth of Gr/ Ni(111)

Figure S1 (panels a and b) shows the real-time evolution of the C 1s core level during the growth of Gr on Ni(111) by dissociation of ethylene at 790 K. For low ethylene dose, the C 1s signal appears at 283.0 eV and is due to a carbide phase, as in Ref. 1. At higher exposure, the Gr phase appears, as evidenced by the emergence of a peak at 284.84 eV, whose intensity becomes predominant while the residual component of carbide species nearly disappears (see C_2 peak in Figure 1a of the main text).

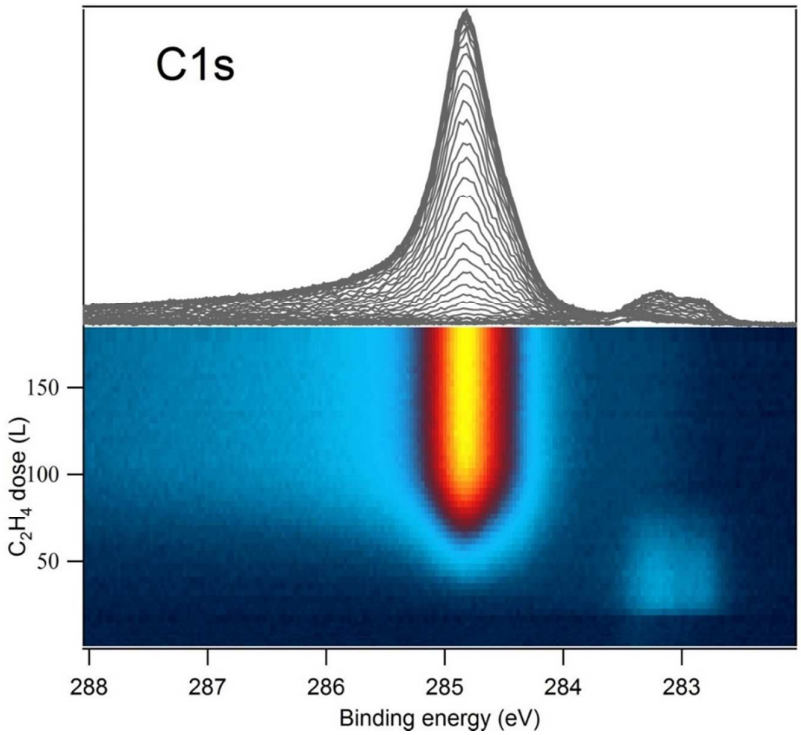

Figure S1. Real-time growth of Gr on Ni(111). Evolution of the C 1s signal during the exposure of the Ni(111) surface to ethylene at 790 K . The photon energy is 400 eV.

S2. Evaluation of the crystalline quality of the grown Gr layer by HAS

HAS is a surface sensitive technique, which provides information about surface structure, as well as on dynamic processes, such as phonons and thin-film growth. Because of the low energies employed (10-100 meV), neutral He atoms probe the topmost surface layer of any material in an inert, completely nondestructive manner.[2] In particular, HAS is characterized by high sensitivity to surface defects, which allows detection of very low adsorbate coverages, down to 0.001 ML.[3] Therefore, it is an incomparable tool to evaluate the crystalline quality of overlayers.[2]

The HAS experiments were performed in Madrid (Spain) with a high-resolution time-of-flight spectrometer, described in detail elsewhere.[4] The He-atom beam is produced in a high-pressure free-jet expansion through a 10 μm nozzle. Measurements reported here were performed with a source pressure P_0 = 70 bar behind the nozzle and at a nozzle temperature of 300 K. The velocity spread of the He beam was estimated to be 3% under these conditions. The base pressure in the scattering

chamber was typically $2x10^{-10}$ mbar, reaching $2x10^{-8}$ mbar with the He beam on. The helium atoms scattered from the sample, after travelling through three differentially pumped stages along the 1.7m long drift tube, are detected by means of a home-made mass sensitive detector. The angle between incident and scattered beam, in a planar geometry, is fixed at a total angle Θ =105.4º. The angular distributions are measured by rotating the crystal by an angle Θ_i around a normal to the plane, defined by the incident and the outgoing beams.

Figure S2 shows a high-resolution HAS pattern measured from a Gr/Ni(111) sample. The specular peak is very sharp, with a FWHM= 0.15º. This corresponds roughly to the angular resolution of the instrument, revealing the good surface quality of the grown Gr layer. Very intense diffraction peaks due to the (1x1) Gr overlayer can be observed. The actual diffraction grating is the periodic modulation of the repulsive part of the He-Gr potential at the energy of the incoming He atoms.

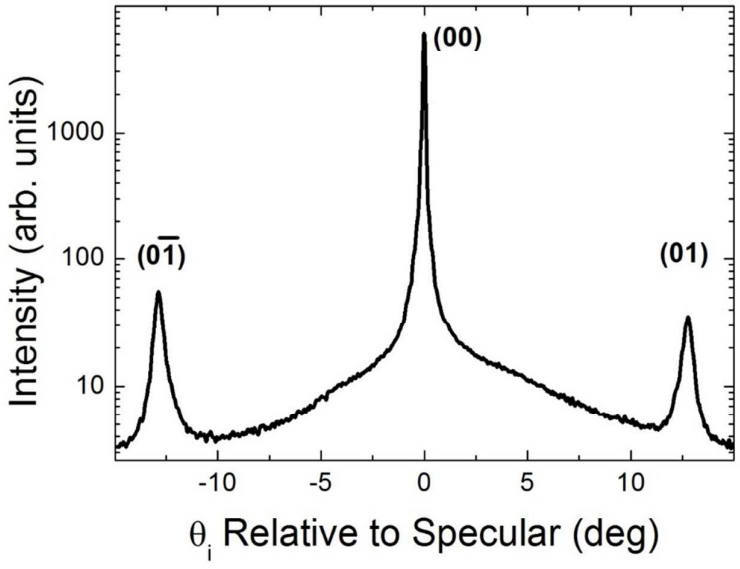

Figure S2. Diffraction pattern of He atoms taken for Gr/Ni(111). Angular distributions of He scattering from the Gr/Ni(111) surface along the ΓM direction. The incident beam energy is 65 meV and the surface temperature is 110 K.

S3. Sticking coefficient of water on Gr/Ni(111) at RT

We have also investigated by means of HAS the adsorption of water on Ni(111) and Gr/Ni(111) at RT. Figure S3 shows the evolution of the specular He intensity as a function of time, measured while dosing water from the background at $p=4x10^{-7}$ mbar. The initial slope of a reflectivity curve (after the beginning of the exposure) is, to first approximation, proportional to the initial sticking coefficient of water molecules.[3] We can estimate a sticking coefficient of $\sim 2 \cdot 10^{-4}$ for H_2O/Ni(111) in our experimental conditions. Our HAS data are consistent with the value of the sticking coefficient determined in Ref. 5. Whereas sticking on clean Ni(111) is revealed by a clear decrease of intensity, a nearly flat curve is measured for Gr/Ni(111). This allows concluding that the initial sticking coefficient of water on Gr/Ni(111) is very low (below 10^{-6}), which provides a clue to understand the very large doses needed to observe the effects reported in the main text of our work. Such a low sticking coefficient cannot be measured by HAS.

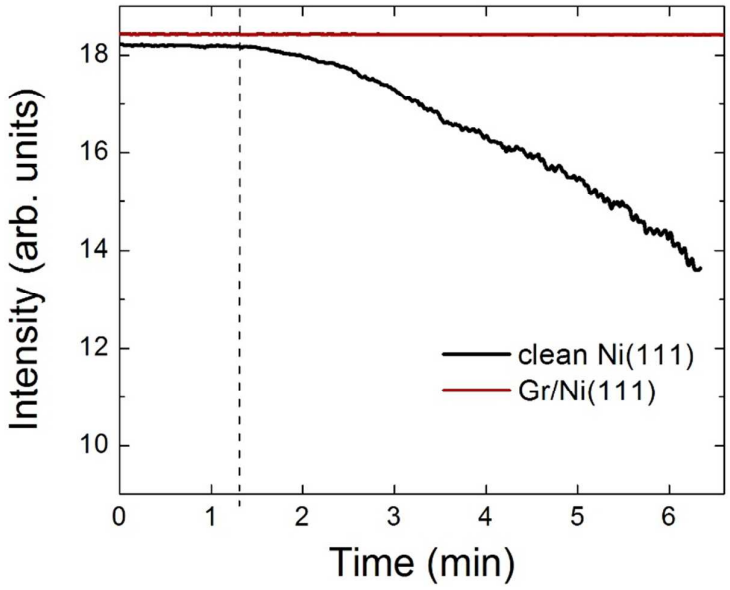

Figure S3. Sticking coefficient of water at RT on Ni(111) and Gr/Ni(111). Intensity of the specularly reflected He beam *versus* time while dosing water at RT on clean Ni(111) (black curve) and Gr/Ni(111) (red curve). The vertical dashed line indicates the opening of the water leak-valve. The decrease of the reflected He intensity for water-dosed Ni(111) is related to the sticking coefficient of water at RT.

S4. Ice formation and desorption in Gr/metals

At a low coverage of water (less than θ=0.03 ML), a singleton-like monomer water molecules have been reported on Ni(111) at 20 K.[6] At higher water coverage (0.03<θ<0.33 ML), ring hexamer like water cluster molecules grew on the surface at wide coverage ranges.

Water clustering on metals begins for T>40 K and becomes extensive above 60 K.[7, 8] Likewise, water clustering has been reported to occur also for Gr epitaxially grown on metals.[9]

The formation of ice on Gr/metals in the temperature range between ~80 and ~130 K has been reported by many groups.[9-13] Ice formation on epitaxial Gr is particularly interesting for the occurrence of metastable hydrophobic wetting two-layer ice.[9] Unlike hexagonal ice, composed by stacks of puckered hexagonal "bilayers", such a novel ice polymorph consists of two flat hexagonal sheets of water molecules in which the hexagons in each sheet are stacked directly on top of each other.

Vibrational spectroscopy is a powerful tool for studying adsorption at surfaces.[14] In particular, the analysis of the vibrational modes of chemisorbed species is not only a fingerprint of the adsorbed chemical species but it also provides information on surface chemical bonds[15] and, moreover, on adsorption geometry.[16]

The vibrational spectrum of ice grown on epitaxial Gr (Figure S4a, red curve) may be divided into four major regions (see Ref. 17 for a review): frustrated translations around 30 meV; frustrated rotations, i.e. librations at 100-110 meV; H_2O deformations, i.e. the scissoring band centered around 200 meV; and O-H stretching modes around 400-460 meV. Instead, the vibrational band around 500 meV should be assigned to a combination mode of the O-H stretching and the libration modes.

By heating the sample to 180 K, ice completely desorbed from Gr, as indicated by the featureless vibrational spectrum (Figure S4a, black curve). Correspondingly, the thermal programmed desorption (TPD) spectrum acquired upon heating ice/Gr/Ni(111) (Figure S4b) shows a desorption peak at 174 K.

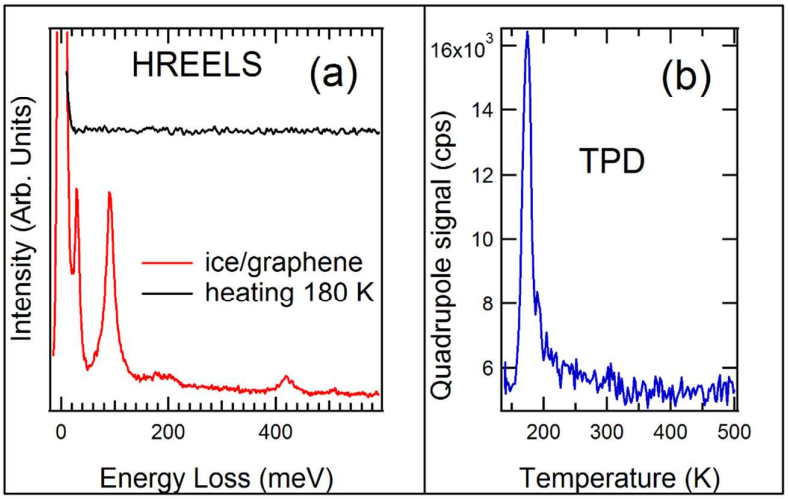

Figure S4. Ice formation and desorption on epitaxial Gr. (a) HREELS spectra for ice grown on epitaxial Gr, before (red curve) and after heating at 180 K (black curve). Both water exposures and HREELS experiments were carried out with the sample kept at 100 K. **(b)** TPD spectra acquired for Gr/Ni(111) exposed to water at 100 K. The ice desorption peak has a maximum at 174 K.

The observation of ice at RT is possible only under very particular situations, as for water locked between two Gr sheets. High-resolution electron microscopy has imaged water sandwiched between two Gr sheets, forming 'square ice', a phase with hydrogen bonding geometry very dissimilar from other water phases.[18] We point out that our experimental conditions are very different.

S5. Analysis of the high-resolution C 1s spectra.

Figure S5 shows the high-resolution C 1s spectra measured on the H_2O-dosed Gr/Ni(111) containing chemisorbed H and intercalated water and on the sample annealed at 470 K and at 750 K. The latter spectrum overlaps completely that measured on the pristine Gr/Ni(111).

In addition to the content of the main text, here we discuss the spectrum measured after the partial annealing at 470 K. According to the XPS, HREELS and TPD results shown in Figures 2 and 4, the sample has completely released H_2 but still contains most of the intercalated water molecules. Thus, the modification of the C1s spectrum taken on this sample with respect to the spectra meas-

ured on the pristine Gr/Ni(111) provides the effect of the intercalated water on Gr. This spectrum is best-fitted with the C_0 and C_1 components at 284.80 and 284.39 eV, as in the pristine Gr, and an additional component (C_5) at 284.31 eV, which, hence, has to be assigned to Gr domains lifted by the intercalated water. The broader line shape of the C_0 component in the presence of intercalated water is an indication of disorder in whole Gr layer. Therefore, we can conclude that the H chemisorption originates the components C_3 and C_4 and shifts C_0 by -0.1 eV, whereas the intercalated water lifts Gr from the substrate and the decoupled domains contribute to the C_5 component.

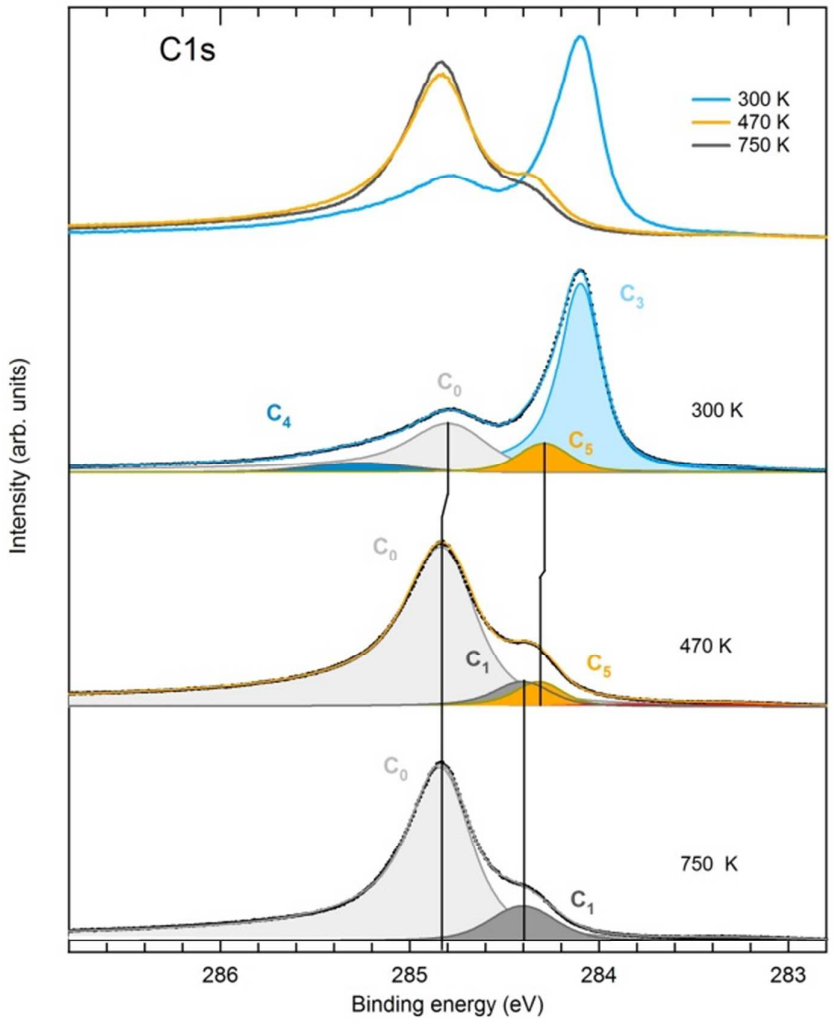

Figure S5. Deconvolution of the C1s spectra taken on the H_2O-dosed Gr/Ni(111) at 300 K and on the sample annealed at 470 K and at 750 K. The spectra are compared at the top of the figure.

S6. Calculations of core-level shifts (cls)

The calculations of C 1s cls were performed by DFT, as implemented in the QUANTUM-ESPRESSO package,[19] using ultrasoft pseudopotentials[20] and the generalized gradient Perdew-Burke-Ernzerhof (PBE)[21] approximation for the exchange-correlation energy functional. A semiempirical dispersion correction[22] was added to improve the description of the interaction between the Gr overlayer and the metallic substrate. The system was modelled using an in-plane 4x6 supercell with the Gr adsorbed on one side of a 5-layers Ni(111) slab. A vacuum region 1.2 nm wide was used to decouple the slab from its periodic replica. The electronic wave functions were expanded in plane waves up to a 45 Ry energy cut-off and a 500 Ry charge density cut-off. The integration over the Brillouin zone was performed using a shifted 8x6x2 Monkhorst-Pack mesh.[23] A Gaussian smearing of 0.02 Ry was used to deal with the metallic character of the system. Atomic positions were relaxed until the forces were below a $1 \cdot 10^{-3}$ a.u. threshold. Cls were calculated in the final-state approximation[24] within the pseudopotential formalism describing the excited atom by a pseudopotential generated in the core excited configuration.

In Figure S6 the C1s cls are reported for a) an ideal (1x1) top-fcc Gr overlayer on Ni(111), b) a defective Gr with four heptagons per 48 atoms on Ni(111) and c) a defective Gr with the same configuration of b) but with two dissociated water molecules intercalated between the Gr and the substrate with one hydrogen and the two -OH groups bound to the substrate and the remaining hydrogen bound to the Gr layer. This latter structure, corresponding to Figure 3c, middle column, of the main text, is reported in the inset of Figure S6c.

Cls are calculated with respect to a free-standing Gr sheet (dashed green line in Figure S6). For the case of an ideal (1x1) top-fcc Gr overlayer on Ni(111), cls are in excellent agreement with previous experimental and theoretical results [25] and, moreover, with our own measurements for the C 1s in pristine Gr/Ni(111) (C_0 and C_1 peaks in the top panel of Figure 1a of the main text).

Note that the bridge-top configuration is also present on the surface, but it has been demonstrated[25] by DFT calculations that the two Gr structures (bridge-top and top-fcc, respectively) show very similar C 1s binding energies.

Results of cls calculations for water-modified Gr/Ni(111) qualitatively indicate a notable red-shift of the binding energies for most of the C atoms, mainly as a consequence of the decoupling between the Gr and the Ni substrate. Experimental results for the C 1s in water-dosed Gr/Ni(111) (C_3 peak in the bottom panel of Figure 1a of the main text) are well reproduced by this model.

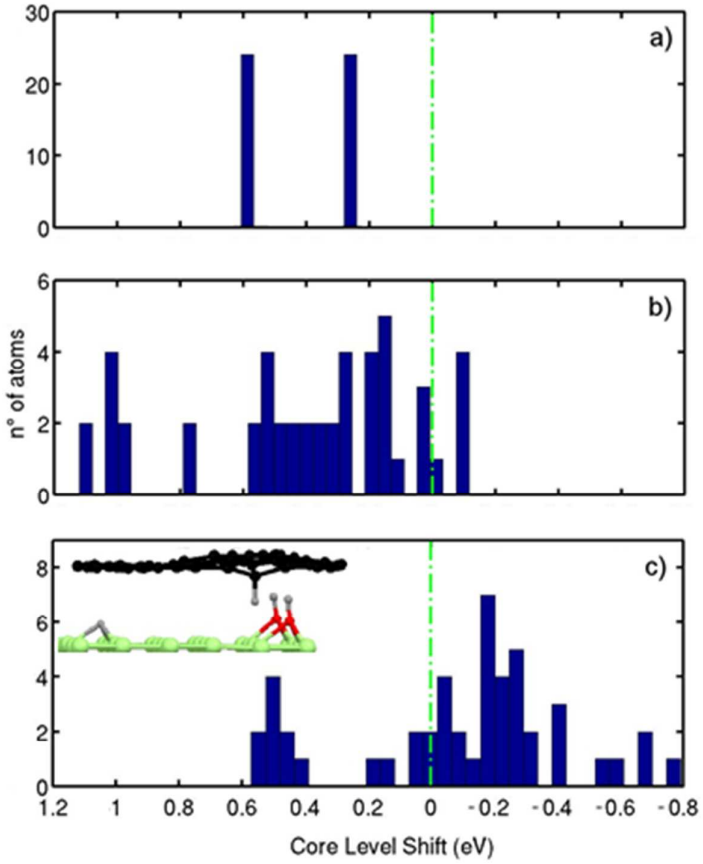

Figure S6. ***Ab initio*** **C 1s cls.** Cls with respect to free-standing Gr for **(a)** ideal (1x1) top-fcc Gr overlayer on Ni(111), **(b)** a defective Gr with four heptagons per 48 atoms on Ni(111) and **(c)** a defective Gr with the same configuration of **(b)** with two dissociated water molecules intercalated between the Gr and the substrate, where one hydrogen atom and the two -OH groups are bound to the substrate and the remaining hydrogen is bound to the Gr layer. The structure is sketched in the inset.

S7. DFT model on water dissociation at RT in Gr/metals

During the optimization, the ion cores were described by norm-conserving non-relativistic pseudo-potentials[26] with cut-off radii 1.14, 1.45, 1.25, 2.15 a.u. for C, O, H and Ni, respectively, and the wave-functions were expanded with localized orbitals and double-ζ basis set for hydrogen and a double-ζ plus polarization basis set for other species. Full optimization of the atomic positions was performed. Optimization of the force and total energy was carried out with an accuracy of 0.04 eV/Å and 1 meV, respectively.

All calculations were carried out with an energy mesh cut-off of 360 Ry and a k-point mesh of 8×6×2 in the Monkhorst-Pack scheme.[26] The optimized distance between the metal substrate and Gr obtained in our calculations agrees with experimental values in literature (see discussion in Ref. 27).

The first step of our DFT modeling is the check of energetics of intercalation process. For the case of pure Gr on nickel substrate, the energy cost of water intercalation is almost the same as the energy cost of desorption of Gr from metallic substrates.[27] This fact evidences the absence of any energy gain from water intercalation between Gr and metallic substrate. The intercalation process is related to Gr delamination energy, which can be estimated by considering the charge transfer from the metallic substrate to Gr (see table S1).

Larger number of Stone-Wales defects provides higher number of carbon atoms located over the outermost layer of the metallic substrate, which affords increasing number of bonds between Gr and substrate. For the estimation of the possible effect of the edges, we performed calculations for the case of Gr nanoribbons over metallic slab but the energy cost of intercalation shows only a slight decrease. Thus, from theoretical results, we can speculate that the main routes for penetration of water between Gr and metals are grain boundaries and defects in the metal substrate, where enough space for migration of water molecules exists and, thus, intercalation start from these areas.

Table S1 Charge transfer from Ni substrate (e^-/C) as a function of defects concentration

Perfect (defect-free)	4 heptagons per 48 carbon atoms	6 heptagons per 48 carbon atoms
0.035	0.042	0.055

Next step of our survey is the modeling of the decomposition of water molecules between the Gr cover and the metal substrate. There are five possible opportunities for decomposition of two water molecules: (1) two hydrogen atoms adsorbed on Gr and two hydroxyl groups adsorbed on the metal substrate (Figure 3b of the main text), (2) hydroxyl groups on Gr and hydrogen on metal, (3) one hydrogen and one hydroxyl group on Gr and same combination on the metallic surface, (4) all hydrogens and hydroxyl groups on Gr or (5) all on the substrate. Our calculations indicate that the energy cost of 4th and 5th combinations is less energetically favorable by about 1.5 eV that the first. Moreover, the 2nd and 3rd combinations are less favorable than the 1st in order of 0.2 eV. This energy difference is weak (about 10% of magnitude) and it depends on the substrate and on the amount of defects. Consequently, the formation of OH-Ni bonds is strongly favored with respect to that of H-Ni bonds. Thus, we can conclude that decomposition of water between Gr and metallic substrate will always provide hydrogenation of Gr. For the case of defect-free Gr, this process is endothermic but, similarly to the case of hydrogenation of free-standing Gr with defects,[28] in this case also Stone-Wales defects make this process exothermic.

Final step of our modeling is the check of stability of hydrogen atoms on Gr. We model two stages of this process: desorption of first (Figure 3c of the main text) and second (Figure 3d of the main text) hydrogen atoms. For the case of pure Gr and lower amount of Stone-Wales defects, the migration of a single hydrogen atom toward the substrate is also exothermic. This result seems rather unusual because the presence of odd number of monovalent species chemisorbed on Gr is much less energetically favorable that even.[29] However, in the case of Gr on metallic substrates, charge transfer from the substrate decreases the energy difference between chemisorption of even and odd num-

ber of monovalent species.[30] For the case of higher amount of Stone-Wales defects, the stable chemisorption of both hydrogen atoms on Gr is more energetically favorable, because the energy gain from chemisorption is proportional to the amount of defects. Desorption of second hydrogen atom from Gr (Figure 3d of main text) is energetically favorable uniquely for defect-free Gr because only in this case the H_2 molecule spontaneously forms in the space between Gr and substrate. For the case of Gr with defects, the migration of both hydrogen atoms to the substrate has an energy cost and, therefore, the formation of H dimers on the metal substrate underneath the Gr cover is unfavorable without providing external energy.

Thus, from results of DFT modeling, we can conclude that, in the vicinity of grain boundaries of Gr on metallic substrate, water molecules will be decomposed to hydrogen and hydroxyl groups and stable hydrogenation of Gr will occur. The amount of hydrogen on Gr and configuration of hydrogenated patterns strongly depends on atomic structure of defects on Gr grain boundaries. The substrate influences the amount of water confined in the space between Gr and the substrate. Conversely, the substrate plays only minor role for the energetics of water decomposition and stability of hydrogen on Gr.

REFERENCES

1. Grüneis, A.; Kummer, K.; Vyalikh, D. V., Dynamics of Graphene Growth on a Metal Surface: a Time-Dependent Photoemission Study. *New J. Phys.* **2009,** *11*, 073050.
2. Farías, D.; Rieder, K. H., Atomic Beam Diffraction from Solid Surfaces. *Rep. Prog. Phys.* **1998,** *61*, 1575-1664.
3. Comsa, G.; Poelsema, B., in *Atomic And Molecular Beam Methods*, Scoles, G., Ed. Oxford University Press: Oxford, 1992; Vol. 2, Pp 463-487.
4. Barredo, D.; Laurent, G.; Nieto, P.; Farías, D.; Miranda, R., High-Resolution Elastic and Rotationally Inelastic Diffraction of D_2 from NiAl(110). *J. Chem. Phys.* **2010,** *133*, 124702.
5. Hundt, P. M.; Jiang, B.; Van Reijzen, M. E.; Guo, H.; Beck, R. D., Vibrationally Promoted Dissociation of Water on Ni(111). *Science* **2014,** *344*, 504-507.
6. Nakamura, M.; Ito, M., Ring Hexamer Like Cluster Molecules of Water Formed on a Ni(111) Surface. *Chem. Phys. Lett.* **2004,** *384*, 256-261.
7. Glebov, A. L.; Graham, A. P.; Menzel, A., Vibrational Spectroscopy of Water Molecules on Pt(111) at Submonolayer Coverages. *Surf. Sci.* **1999,** *427-428*, 22-26.
8. Daschbach, J., Adsorption, Desorption, and Clustering of H_2O on Pt(111). *J. Chem. Phys.* **2004,** *120*, 1516.

9. Kimmel, G. A.; Matthiesen, J.; Baer, M.; Mundy, C. J.; Petrik, N. G.; Smith, R. S.; Dohnálek, Z.; Kay, B. D., No Confinement Needed: Observation of a Metastable Hydrophobic Wetting Two-Layer Ice on Graphene. *J. Am. Chem. Soc.* **2009,** *131*, 12838-12844.
10. Politano, A.; Chiarello, G., The Nature of Free O-H Stretching in Water Adsorbed on Carbon Nanosystems. *J. Chem. Phys.* **2013,** *139*, 064704-4.
11. Politano, A.; Chiarello, G., Ice Formation on Clean and Alkali-Doped Quasi-Freestanding Graphene: a Vibrational Investigation. *Carbon* **2015,** *93*, 242-249.
12. Politano, A.; Marino, A. R.; Formoso, V.; Chiarello, G., Hydrogen Bonding at the Water/Quasi-Freestanding Graphene Interface. *Carbon* **2011,** *49*, 5180-5184.
13. Smith, R. S.; Matthiesen, J.; Kay, B. D., Desorption Kinetics of Methanol, Ethanol, and Water from Graphene. *J. Phys. Chem. A* **2014,** *118*, 8242–8250.
14. Politano, A.; Chiarello, G.; Benedek, G.; Chulkov, E. V.; Echenique, P. M., Vibrational Measurements on Alkali Coadsorption Systems: Experiments and Theory. *Surf. Sci. Rep.* **2013,** *68*, 305–389.
15. Politano, A.; Chiarello, G., Vibrational Investigation of Catalyst Surfaces: Change of the Adsorption Site of CO Molecules Upon Coadsorption. *J. Phys. Chem. C* **2011,** *115*, 13541-13553.
16. Lopez, A.; Bitzer, T.; Heller, T.; Richardson, N. V., Functional Group Selectivity in Adsorption of 4-Aminobenzoic Acid on Clean and Na Modified Si(100)-2×1 Surfaces. *Surf. Sci.* **2001,** *480*, 65-72.
17. Henderson, M. A., The Interaction of Water with Solid Surfaces: Fundamental Aspects Revisited. *Surf. Sci. Rep.* **2002,** *46*, 1-308.
18. Algara-Siller, G.; Lehtinen, O.; Wang, F. C.; Nair, R. R.; Kaiser, U.; Wu, H. A.; Geim, A. K.; Grigorieva, I. V., Square Ice in Graphene Nanocapillaries. *Nature* **2015,** *519*, 443-445.
19. Giannozzi, P.; Baroni, S.; Bonini, N.; Calandra, M.; Car, R.; Cavazzoni, C.; Ceresoli, D.; Chiarotti, G. L.; Cococcioni, M.; Dabo, I.; Dal Corso, A.; De Gironcoli, S.; Fabris, S.; Fratesi, G.; Gebauer, R.; Gerstmann, U.; Gougoussis, C.; Kokalj, A.; Michele, L.; Martin-Samos, L.; Marzari, N.; Mauri, F.; Mazzarello, R.; Paolini, S.; Pasquarello, A.; Paulatto, L.; Sbraccia, C.; Scandolo, S.; Sclauzero, G.; Seitsonen, A. P.; Smogunov, A.; Umari, P.; Wentzcovitch, R. M., QUANTUM ESPRESSO: a Modular and Open-Source Software Project for Quantum Simulations of Materials. *J. Phys.: Condens. Matter* **2009,** *21*, 395502.
20. Vanderbilt, D., Soft Self-Consistent Pseudopotentials in a Generalized Eigenvalue Formalism. *Phys. Rev. B* **1990,** *41*, 7892-7895.
21. Perdew, J. P.; Burke, K.; Ernzerhof, M., Generalized Gradient Approximation Made Simple. *Phys. Rev. Lett.* **1996,** *77*, 3865-3868.
22. Grimme, S., Accurate Description of Van der Waals Complexes by Density Functional Theory Including Empirical Corrections. *J. Comput. Chem.* **2004,** *25*, 1463-1473.
23. Monkhorst, H. J.; Pack, J. D., Special Points for Brillouin-Zone Integrations. *Phys. Rev. B* **1976,** *13*, 5188-5192.
24. Bianchettin, L.; Baraldi, A.; De Gironcoli, S.; Lizzit, S.; Petaccia, L.; Vesselli, E.; Comelli, G.; Rosei, R., Geometric and Electronic Structure of the N/Rh(100) System by Core-Level Photoelectron Spectroscopy: Experiment and Theory. *Phys. Rev. B* **2006,** *74*, 045430.
25. Zhao, W.; Kozlov, S. M.; Höfert, O.; Gotterbarm, K.; Lorenz, M. P. A.; Viñes, F.; Papp, C.; Görling, A.; Steinrück, H.-P., Graphene on Ni(111): Coexistence of Different Surface Structures. *J. Phys. Chem. Lett.* **2011,** *2*, 759-764.
26. Troullier, N.; Martins, J. L., Efficient Pseudopotentials for Plane-Wave Calculations. *Phys. Rev. B* **1991,** *43*, 1993-2006.
27. Boukhvalov, D. W.; Gornostyrev, Y. N.; Uimin, M. A.; Korolev, A. V.; Yermakov, A. Y., Atomic, Electronic and Magnetic Structure of Graphene/Iron and Nickel Interfaces: Theory and Experiment. *RSC Advances* **2015,** *5*, 9173-9179.
28. Boukhvalov, D. W.; Katsnelson, M. I., Chemical Functionalization of Graphene with Defects. *Nano Lett.* **2008,** *8*, 4373-4379.
29. Galakhov, V. R.; Buling, A.; Neumann, M.; Ovechkina, N. A.; Shkvarin, A. S.; Semenova, A. S.; Uimin, M. A.; Yermakov, A. Y.; Kurmaev, E. Z.; Vilkov, O. Y.; Boukhvalov, D. W., Carbon States in Carbon-Encapsulated Nickel Nanoparticles Studied by Means of X-Ray Absorption, Emission, and Photoelectron Spectroscopies. *J. Phys. Chem. C* **2011,** *115*, 24615-24620.

30. Boukhvalov, D. W.; Son, Y. W.; Ruoff, R. S., Water Splitting Over Graphene-Based Catalysts: *ab Initio* Calculations. *ACS Catalysis* **2014,** *4*, 2016-2021.